

PROCEEDINGS OF SPIE

SPIDigitalLibrary.org/conference-proceedings-of-spie

Hyperion: Far-UV cross dispersion spectroscopy design

Choi, Heejoo, Trumper, Isaac, Feng, Yi-Ting, Kang, Hyukmo, Hamden, Erika, et al.

Heejoo Choi, Isaac Trumper, Yi-Ting Feng, Hyukmo Kang, Erika Hamden, Dae Wook Kim, "Hyperion: Far-UV cross dispersion spectroscopy design," Proc. SPIE 11487, Optical Manufacturing and Testing XIII, 114870W (20 August 2020); doi: 10.1117/12.2570489

SPIE.

Event: SPIE Optical Engineering + Applications, 2020, Online Only

Hyperion: Far-UV cross dispersion spectroscopy design

Heejoo Choi^{1,2}, Isaac Trumper^{1,3}, Yi-Ting Feng¹, Hyukmo Kang¹, Joel Berkson¹,
Erika Hamden⁴, and Dae Wook Kim^{1,2,4,*}

¹Wyant College of Optical Sciences, University of Arizona, 1630 E. University Blvd., Tucson, AZ 85721, USA

²Large Binocular Telescope Observatory, University of Arizona 933 N Cherry Avenue, Tucson, AZ 85721, USA;

³ELE Optics, Inc., 405 E. Wetmore Ste 117-260, Tucson, AZ 85705, USA;

⁴Department of Astronomy and Steward Observatory, University of Arizona, 933 N. Cherry Ave., Tucson, AZ 85721, USA

ABSTRACT

Hyperion is a far-UV mission that investigates the birth clouds of stars using a 40 cm aperture telescope feeding an imaging long-slit spectrometer. The science requirements of the mission dictate that the spectrometer covers 140.5-164.5 nm spectral range with resolution greater than 30,000. We employ smart and efficient design to create a long-slit, cross dispersed, echelle spectrometer that utilizes a two-mirror freeform imaging optics. Echelle spectra for $n = -19, -18,$ and -17 over a $10 \text{ arcmin} \times 2.5 \text{ arcsec}$ (length \times width) FFOV are imaged onto the focal plane. We simulate the optical performance and the expected spectral efficiency.

Keywords: space telescope, far-UV spectroscopy, échelle grating, freeform optic

1. INTRODUCTION

The scientific goal of the UV space telescope Hyperion is to examine the fuel for star formation (SF) by probing the nature, extent, and state of H₂ at the crucial atomic-to-molecular interstellar medium boundary layer^{1,2,3}. The telescope apparatus must observe from above Earth's UV-blocking atmosphere because the target spectral band (UV-H₂) could be absorbed by the atmosphere. These measured physical parameters uncover the relationship between SF, cloud evaporation in the presence of a radiation field, and how a forming star itself impacts SF efficiency across galactic star-forming regions. Hyperion examines the fuel for star formation directly by observing the molecular interface between dense, star-forming clouds, the diffuse interstellar environment, and the stars that arise from these regions.

The optical performance requirement of the Hyperion mission is 5 arcsec spatial resolution, 10 arcmin instantaneous field of view (FOV), $R > 30,000$ spectral resolution (i.e., $\lambda/\Delta\lambda$), and photometric resolution at 2 %. We adopted δ -doped charge-coupled devices (CCDs)^{4,5} with a combination of an échelle grating, cross-dispersion, and a freeform optics imaging system to meet the science requirements. Especially, the requirement of the science-driven specification and the space of the bus adds complexity to the telescope design. In the last couple of decades, researchers and scientists have accomplished UV observation space telescopes, with Galaxy Evolution Explorer (GALEX)^{6,7,8} and Far Ultraviolet Spectroscopic Explorer (FUSE)^{9,10} as outstanding representative missions. GALEX utilized a dichroic beam splitter combined with a grism, and FUSE used a four-segmented Rowland circle layout that has been adopted for spacecraft spectroscopy^{11,12,13}. If the detectors can be installed at the curved Rowland circle, and a relatively narrow spectral range is required, the Rowland design's compact and low spectral aberration are an attractive advantage. Multiple sets of cascaded Rowland spectrometers can be adopted to cover broad spectrums as FUSE did.

However, the desired spectral resolution imaging quality of Hyperion cannot be achieved by traditional cross-dispersion spectroscopy design methods such as a grating combined with a prism, therefore the optical design requires more creative solutions. We present an enabling design solution using an on-axis and in-plane diffractive optics layout enabling intuitive aberration control by using cross-dispersion Type-4 freeform configuration¹⁴.

*E-mail: letter2dwk@hotmail.com

Optical Manufacturing and Testing XIII, edited by Dae Wook Kim, Rolf Rascher,
Proc. of SPIE Vol. 11487, 114870W · © 2020 SPIE · CCC code:
0277-786X/20/\$21 · doi: 10.1117/12.2570489

This paper presents the Hyperion optical design as follows. In section 2. The requirement of optical design is elaborated, and our solution to meet the demand is presented in section 3. The results of geometric optical analysis and physical wave propagation are described in section 4.

2. OPTICAL DESIGN GUIDELINES

2.1 High dynamic-range of detector

The detector array of the telescope defines the measurable spectral range due to the bandgap of the doped materials in semiconductors, which limits the space mission's measurable objects. Hyperion's target is a far-ultraviolet (FUV) spectrum, but the usual Si-based detector array will not see this spectrum. The microchannel plate (MCP) has been used for FUV missions before, but it has many limitations such as low quantum efficiency, low dynamic range, and limited spectral band and stability.

These challenges have been overcome thanks to NASA technology developments^{4, 5}. The δ -doped CCDs, developed by JPL (Jet Propulsion Laboratory) scientists, allow the high-resolution emission measurement of UV-H₂. The δ -doped CCDs have good efficiency in the UV, with the application of specialized anti-reflection coatings. The Hyperion design uses a simple MgF₂ coating to achieve > 55 % QE in the bandpass.

The higher dynamic range of a CCD means that we have the ability to measure from bright to dim objects. Additionally, the fabrication and operation of the δ -doped CCDs are more relaxed and inexpensive than MCP with respect to prices and power requirements. The dimension specification we used for optical design is; array dimension 49.1 × 49.1 mm, with 4095 × 4095 pixels (12 μ m pitch).

2.2 High spectral resolution instrument in compact form factor

In basic spectroscopy design, three primary groups of optical components are used: collimation, dispersion, and imaging optics. Collimating the light from the input slit to the grating is relatively easy compared to imaging because the inserted beam is usually close to a point source or only a single dimension field of view (slit), which can be collimated without significant field aberrations by means of a concave mirror (e.g., off-axis parabolic mirror). When the light starts to disperse into a wide diffractive angle after the collimated beam interacting with the grating, the imaging optics group needs to accommodate this large chromatic field of view while minimizing aberration. The high spectral resolution R ($\lambda/\Delta\lambda$) design usually has a fast divergence diffractive angle and raises distortion of the slit imaging⁷.

In order to have higher resolution spectrometer design, there are three general techniques, 1) long propagation after the grating, 2) higher groove density or higher diffraction order, and 3) high-resolution imaging systems and sensors.

The long propagation requires a large volume or multi-folding mirror for the optical layout. This is challenging to space optics design due to the limitation of the volume and mass limit of the bus. The second option means that the imaging optics design will encounter a more extensive chromatic field acceptance, which greatly challenges the optical design. Finally, the pixel pitch of the sensor is defined by the semiconductor manufacturing process. A better imaging system for small spots on the sensor, and a wide field of view for a diffractive beam after the grating, would be a promising solution for a high-resolution spectrometer in a space mission.

3. ÉCHELLE AND FREEFORM OPTICAL DESIGN FOR HYPERION

3.1 Overall optical layout of the échelle cross-dispersion spectrometer

Hyperion has adopted a significantly longer slit length than previous missions (GALEX or FUSE) for spatial FOV. The extreme aspect ratio of the long-slit (10 arcmin × 2.5 arcsec, aspect ratio of 240) and the very high spectral resolution requirement ($R > 30,000$) at the FUV spectral range (1405 Å – 1645 Å) make the optical design of Hyperion unique by utilizing the freeform and cross-dispersion configuration design approach.

In order to achieve this high spectral resolution, we used a non-traditional method with two consecutive gratings for diffractive optics and chose high diffraction orders (Fig. 1). The Ritchey-Chrétien telescope design (i.e., hyperbolic mirror for primary and secondary) is adopted to cover 10 arcmin field of view. The telescope apparatus passes the F/6 (effective focal length EFL = 2400 mm) beam to the spectrometer instrument.

In traditional spectrometer design, the inserted beam hits the collimating mirror on-axis and it deviates to a planar grating placed off-axis. This design could induce aberration in spectral and slit imaging. We resolved the aberration

issue by adopting annular type échelle grating and placing the slit on-axis of the telescope to create a normal incidence angle to the échelle grating, as shown in Fig. 1 (a). Because of the annular pupil of the Ritchey-Chrétien, caused by the secondary obstacle, the center hole approach does not induce any photon loss for all field cases.

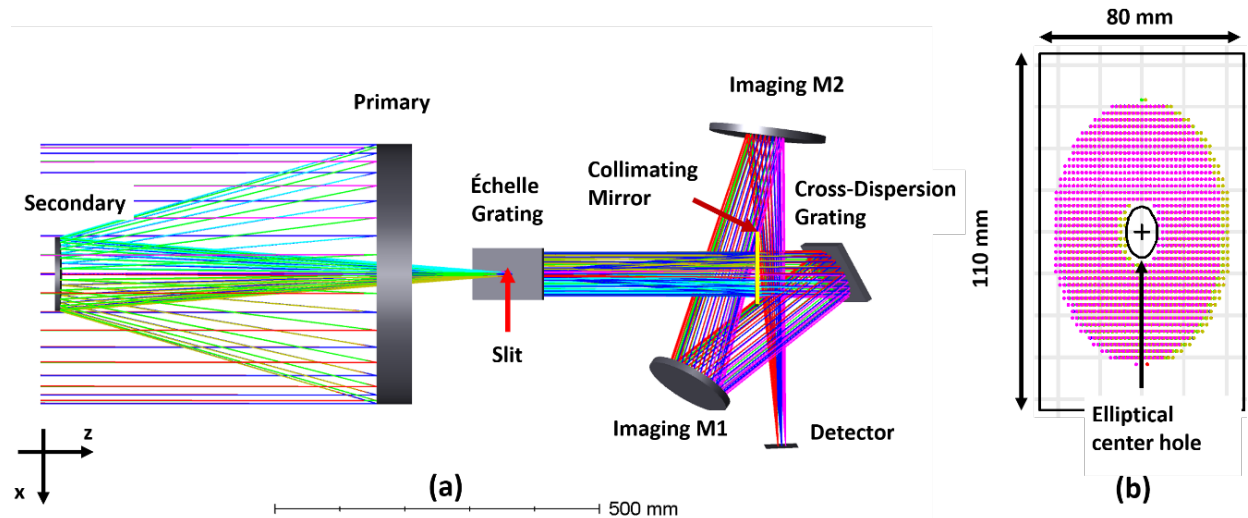


Fig. 1. The overall layout of the Hyperion UV space telescope and footprint diagram of all fields on centerholed échelle grating. (a) The slit is uniquely placed at the échelle grating center hole. Thanks to the central hole of the échelle grating, the collimator and échelle grating can be placed on-axis to minimize the aberration. The diffraction angle of the échelle and cross-dispersion are orthogonal to each other. (b) Annular type échelle grating with a central hole (matching the secondary mirror obscuration) allows the unique on-axis optical layout without photon loss.

The diffractive angle of the target spectral range (1405 – 1645 Å) on both grating surfaces are 5° at the first échelle grating and 3.8° at the second cross-dispersion grating. The freeform imaging optics should make spots on the $50\text{ mm} \times 50\text{ mm}$ δ -doped CCD sensor from the $\sim 104\text{ mm} \times 68\text{ mm}$ ellipse pupil, and divergences of 5° and 3.8° from the two different conjugate planes. The broadening spot on the sensor means not only the loss of spatial but also spectral resolution.

3.2 Compact Type-4 freeform imaging optics layout

To accommodate a large cross-dispersed FOV while maintaining a small focused spot, a freeform two-mirror imaging system (M1 and M2) was designed and optimized as an actual design application of the previously reported Type-4 design form approach¹⁴.

Rotationally symmetric systems were not feasible in this instrument because of the constraint on volume. A three-mirror design would provide better imaging performance^{15,16}, but this would come at the expense of a larger volume requirement, as well as photon loss from the extra reflector.

The two-mirror system employs a Type-4 design form, which supports a large FOV in a compact volume, a critical factor for space missions. Furthermore, the use of the échelle grating on-axis means that all the dispersive elements (collimator, échelle grating, and cross-dispersion grating) can be placed along the same optical axis, reducing off-axis aberrations^{17,18}.

The two-mirror Type-4 system can then have its folding direction along the same plane, leveraging more straightforward aberration behavior for better optical performance. To accommodate the planar anamorphism at the échelle grating and rectangular field width of the slit, the collimator was specified with a bi-conic surface, which improves the pupil quality and reduces the aberration burden on the imaging system. The Type-4 form supports a significant separation between its entrance pupil and the first mirror, easily accommodating the pupil matching requirement. The imaging optics in the Type-4 layout are specified with Zernike polynomials (order up to the 50th term in Noll ordering). The telescope and ray relay optics design values are summarized in Table 1 as a reference for those who want to benchmark or reproduce the design.

Table 1. Hyperion optical design values and component characteristics

Parameters	Values
Telescope	
Primary mirror diameter (M1)	40 cm
Secondary Mirror diameter (M2)	12.5 cm
F-number / EFL	6 / 240 cm
Imaging optics (M4&M5)	
Primary imaging optic (M4)	Freeform (up to 50 th term Standard Zernike polynomials)
Secondary imaging optic (M5)	Freeform (up to 50 th term Standard Zernike polynomials)
Working F-number	8

4. OPTICAL PERFORMANCE ANALYSIS

4.1 Spectral and spatial resolution performance

The image performance was evaluated with full-spectrum and full-field images. Six field points (four corners and two at the middle top and bottom) were defined to match the actual Hyperion slit size. The spot sizes for all fields and wavelengths are the first elements for optical performance evaluation. We selected the line per unit length (groove) and the diffractive order of both gratings to cover the full spectrum within the given detector size in 2D formation. The full cross-dispersed spectra are shown in Fig. 2.

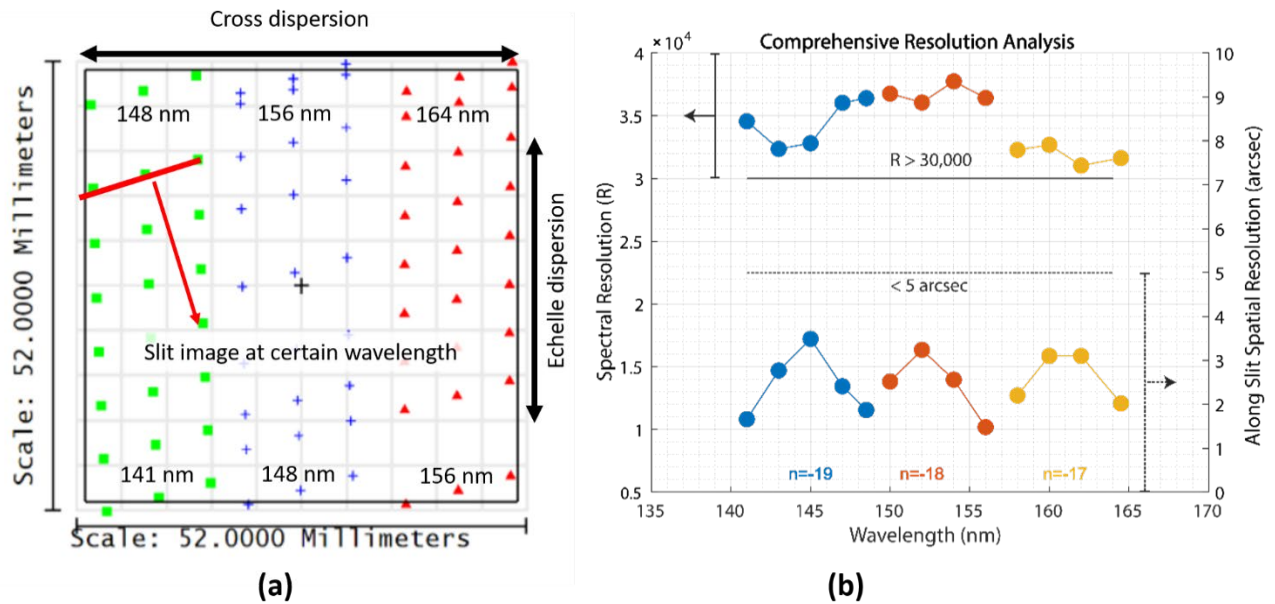


Fig. 2. (a) Spectrum distribution on the detector sensor plane, and (b) Comprehensive spectral resolution plot. The dispersion along the vertical is from the échelle grating, and the horizontal dispersion (three stripes) is from two consecutive cross-dispersion gratings. Each field image on the sensor is confined in a small spot to meet $R > 30,000$.

The blurred slit image overlapping with neighboring with adjacent wavelength slit image induces the loss of spectral resolution. To achieve a small spot, we optimized to get the clearly separated spectral stripes on the sensor, and then the imaging optics were optimized to obtain a well-confined slit image of the six fields. We compromised first and second steps to create tight spot sizes at the edges of the spectral band (at the corners of the detector) with the need to optimize the fields near the center.

In order to verify the spectral resolution of the design, we used a distinct minimum wavelength step as a criterion. We insert the target λ , and $\lambda + \Delta$ (5 pm), and analyze whether both slit images from those wavelengths are distinguishable. The target spectral resolution is $R > 30,000$, corresponding to a spectral resolution of ~ 5 pm (picometer). The perimeter slit images also show equal quality over the entire detector array. The spatial resolution along the slit is < 5 arcsec for all fields and wavelengths, as the comprehensive resolution plot shows in Fig. 2 (b).

4.2 Diffraction efficiency performance

A grating simulation using the sequential ray-tracing method has limitations when calculating the entire physical phenomena of diffraction. The number of grooves on the grating and its order are the only parameters used in sequential ray trace and optimization for optical relay design. The wave propagation approach is adequate for detailed grating simulation to understand all the physical phenomena of diffraction. The efficiency over the spectrum and corresponding blaze angles are fundamental inputs to evaluate the yield of FUV susceptibility and feasibility of the design.

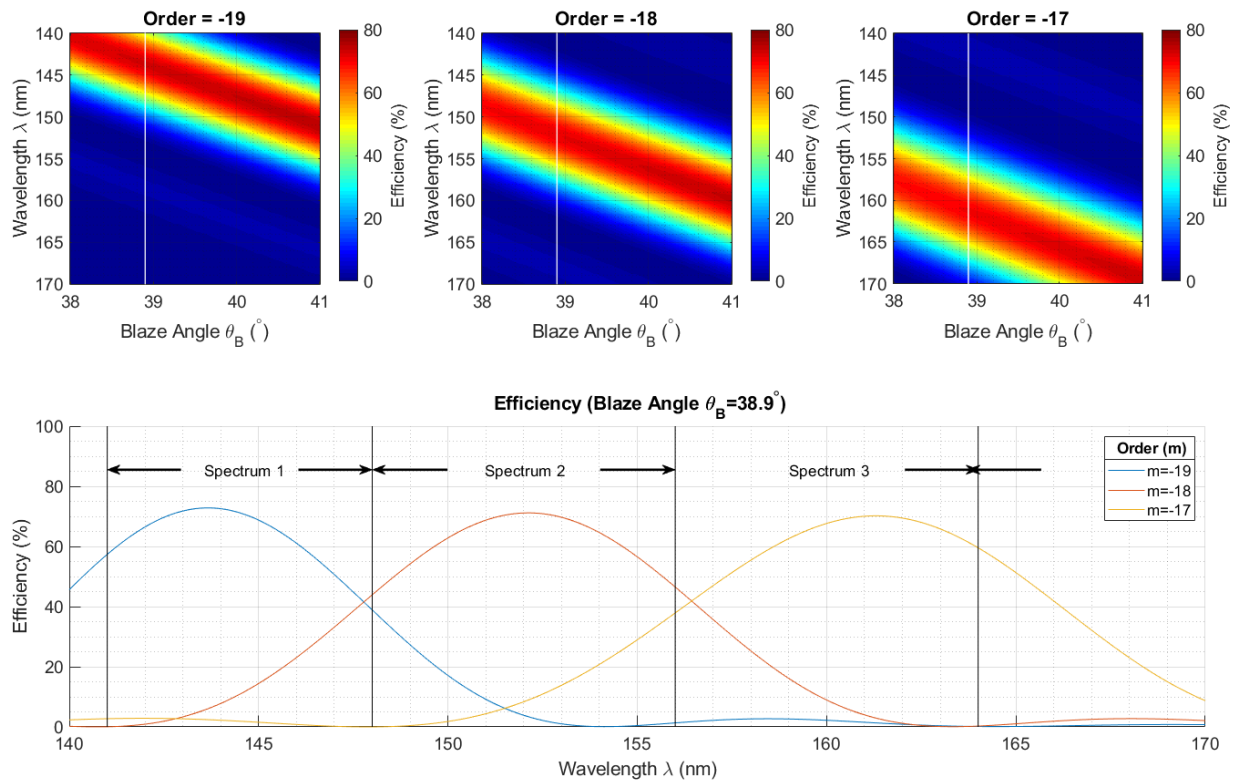


Fig. 3. The diffraction efficiency simulation of échelle grating. (a)–(c) The 2D efficiency plot for each diffraction order with blaze angle vs. wavelength. We determine the blaze angle to have even efficiency for all three spectrum stripes, and it was determined as 38.9° (The white line in the plot.) (d) The overall efficiency of the full spectrum. The spectrums 1–3 correspond to diffraction orders of -19, -18 and -17, respectively.

The divergence angle of the spectrum is fast at high order, and this is beneficial for spectral resolution. However, as shown in Fig. 3 (a) – (c), the efficiency rapidly declines over the spectrum. At the high order, the chosen blaze angle focuses the energy in a certain direction, it is usually narrow than low order and it causes a lower of photons efficiency at boundary wavelength. We selected the blaze angle (38.9° , illustrated by the white vertical line in Fig. 3 (a) – (c)) while considering the incidence angle to the grating so that the three orders have even efficiency. Because of the cross-dispersion approach, there is no issue with the overlapping in the free spectral range of the three orders where they have similar efficiency over the entire target spectrum range.

The essential role of the second grating is to isolate each band clearly at the detector plane. It uses a single diffraction order to separate overlapping stripes from the first échelle grating by leveraging a wide free spectral range. Moreover, the low order has flat efficiency for the entire spectral range with the selected single order. Based on the numerical calculation, we chose the -1 order, and then we surveyed the blaze angle. We selected the blaze angle at 13.275° . We

used the chief ray of the center field to evaluate the incidence angle to the grating. The combined FUV throughput from both dispersive optics is estimated to be > 30 %. The diffractive optics specification is elaborated in Table 2 for reference.

Table 2. Hyperion diffractive optics design values

Parameters	Values
Spectrometer	
Wavelength Range	140.5 –164.5 nm
Entrance Slit, FOV width	2.5 arcsec
Entrance Slit, FOV height	10 arcmin
Slit width on detector	2.083 pixels
Wide slit (×2)	20 arcsec × 30 arcsec
Collimating Optic (M3), Biconic	$f_{lx} = 799 \text{ mm}$ Conic _x = -0.55 $f_{ly} = 800 \text{ mm}$ Conic _y = -1.4828
Échelle grating (EG), planar grating	
Aperture Size	80 mm × 110 mm
α (incidence angle), β (diffractive angle), blaze angles	50 °, 35 °, 38.9 °
échelle grating groove density	450 lines/mm
Operating orders	n = -19, -18, and -17
Cross dispersing grating	
Aperture size	100 mm × 150 mm
α , β , blaze angles	30 °, 10 °, 13.275 °
Cross Disperser groove density	2600 lines/mm
Operating order	n = -1

In the real situation, all diffraction orders are also present in the spectrometer and were not evaluated at the sensor plane in the performance analysis above. For stray light mitigation in the design of the spectrometer, we deliberately positioned the optics and adjusted the incidence and diffractive angles so that the unwanted diffractive rays do not have a direct path to the remaining optical components. In the spectrometer box, the mirror back surface and grating mount, spectrometer box, and sensor package may cause the reflection of the unwanted beam. With conventional black coatings and/or baffle designs can be performed using a non-sequential ray-tracing analysis to reduce out-of-band light leakage.

5. CONCLUSION

The high spectral resolution space telescope for Hyperion mission is designed and analyzed. The δ -doped CCDs, developed by JPL, extend the measurable UV range to 141 nm. We adopted the on-axis layout of the telescope apparatus and in-plan design using annular type échelle grating to allows for intuitive aberration control with type-4 imaging optics layout. This new approach ensures a spectral resolution of $R > 30,000$, and a spatial resolution of 3 arcsec. The geometric optics design and spectral properties were implemented and evaluated, and the first version of the Hyperion FUV telescope design was found to thoroughly address the scientific requirements. We wish that our design approach and parameters are a reference and benchmark of FUV cross-dispersion design. Hyperion was submitted to the SMEX 2019 AO and was not selected. The Hyperion team is planning to revise the mission for the 2021 MIDEX call.

ACKNOWLEDGEMENT

The authors would like to thank the Technology Research Initiative Fund (TRIF) Optics/Imaging Program, through the Wyant College of Optical Sciences at the University of Arizona and the Friends of Tucson Optics (FoTO) Endowed Scholarships in Optical Sciences.

REFERENCES

- [1] Decataldo, D., A. Pallottini, A. Ferrara, Livia Vallini, and S. Gallerani. "Photoevaporation of Jeans-unstable molecular clumps." *Monthly Notices of the Royal Astronomical Society* 487, no. 3, 3377-3391 (2019).
- [2] Gould, R. J., and Salpeter, E. E., "The Interstellar Abundance of the Hydrogen Molecule. I. Basic Processes." *ApJ* 138, 393 (1963).
- [3] Krumholz, Mark R., "The big problems in star formation: the star formation rate, stellar clustering, and the initial mass function." *Physics Reports* 539(2), 49-134 (2014).
- [4] Hoenk, M. E., Grunthaler, P.J., Grunthaler, F.J., Terhune, R. W., Fattahi, M., Tseng, H-F., "Growth of a delta-doped silicon layer by molecular beam epitaxy on a charge-coupled device for reflection-limited ultraviolet quantum efficiency." *Applied Physics Letters* 61(9), 1084-1086 (1992).
- [5] Nikzad, S., Hoenk, M.E., Greer, F., Jacquot, B., Monacos, S., Jones, T.J., Blacksberg, J., Hamden, E., Schiminovich, D., Martin, C., Morrissey, P., "Delta-doped electron-multiplied CCD with absolute quantum efficiency over 50% in the near to far ultraviolet range for single photon counting applications." *Applied Optics* 51(3), 365-369 (2012).
- [6] Morrissey, P., "A GALEX instrument overview and lessons learned," *Proc. SPIE* 6266, *Space Telescopes and Instrumentation II: Ultraviolet to Gamma Ray*, 62660Y (13 June 2006).
- [7] Grange, R., Milliard, B., Flamand, J., Pauget, A., Waultier, G., Moreaux, G., Rossin, C., Viton, M., Nevriere, N., "GALEX UV grism for slitless spectroscopy survey," *Proc. SPIE* 10569, *International Conference on Space Optics — ICSO 2000*, 1056908 (21 November 2017).
- [8] Wyder, T. K., Treyer, M.A., Milliard, B., Schiminovich, D., Arnouts, S., Budavári, T., Barlow T.A., Bianchi, L., Byun, Y-I., Donas, J., "The ultraviolet galaxy luminosity function in the local universe from GALEX data." *The Astrophysical Journal Letters* 619(1), L15 (2005).
- [9] Content, D.A., Davila, P.S., Osantowski, J.F., Saha, T.T., Wilson, M.E., Friedman, S.D., "Optical design of Lyman/FUSE", *Proc. SPIE* 1235, *Instrumentation in Astronomy VII*, (1 July 1990);
- [10] McCandliss, S.R. "Molecular hydrogen optical depth templates for FUSE data analysis." *Publications of the Astronomical Society of the Pacific* 115(808), 651 (2003).
- [11] Hurwitz, M., and Bowyer, S., "A High Resolution Spectrometer For EUV/FUV Wavelengths," *Proc. SPIE* 0627, *Instrumentation in Astronomy VI*, (13 October 1986).
- [12] Harada, T., Sakuma, H., Takahashi, K., Watanabe, T., Hara, H., Kita, T., "Design of a high-resolution extreme-ultraviolet imaging spectrometer with aberration-corrected concave gratings," *Appl. Opt.* 37, 6803-6810 (1998)
- [13] Green, J.C., Wilkinson, E., Friedman, S.D., "Design of the Far Ultraviolet Spectroscopic Explorer spectrograph," *Proc. SPIE* 2283, *X-Ray and Ultraviolet Spectroscopy and Polarimetry*, (7 November 1994).
- [14] Trumper, I., [Anderson](#), A.Q., [Howard](#), J.M., [West](#), G., [Kim](#), D.W., "Design form classification of two-mirror unobstructed freeform telescopes." *Optical Engineering* 59(2) 025105 (2020).
- [15] Bauer, A., Schiesser, E.M., Rolland, J.P., "Starting geometry creation and design method for freeform optics." *Nature Communications* 9, 1756 (2018).
- [16] Papa, J.C., Howard, J.M., Rolland, J.P., "Three-mirror freeform imagers," *Proc. SPIE* 10690, *Optical Design and Engineering VII*, 106901D (21 June 2018).
- [17] Smith, W.J., "Modern lens design." New York: McGraw-Hill, (2005).
- [18] Shannon, R.R., "The art and science of optical design." Cambridge University Press, 1997.